Atomic Layer Deposition Assisted Template Approach for Electrochemical Synthesis of Au Crescent-Shaped Half-Nanotubes

Yong Qin,*,‡ Anlian Pan,§ Lifeng Liu,‡ Oussama Moutanabbir,‡ Ren Bin Yang,‡ and Mato Knez*,‡

‡Max Planck Institute of Microstructure Physics, Halle 06120, Germany, and §College of Physics and Microelectronics Science, Key Laboratory for Micro-Nano Physics and Technology of Hunan Province, Hunan University, Changsha 410082, People's Republic of China

ABSTRACT This paper reports on a novel and versatile method to synthesize sharp-edged crescent-shaped half-nanotubes (HNTs) using a flexible template-based nanofabrication method assisted by atomic layer deposition. This was achieved by electrodeposition inside crescent-shaped nanochannels created by a controlled removal of a sacrificial layer, which was deposited by atomic layer deposition onto the pore walls of an anodic aluminum oxide template. This method provides a high degree of freedom in the manipulation of the morphological properties of HNTs such as the edge sharpness, opening, gap size, and the wall thickness. Initial optical investigations of the HNTs reveal distinct surface plasmon resonance by dark field scattering spectra and surface enhanced Raman spectrum.

KEYWORDS: atomic layer deposition · half-nanotube · sacrificial materials · plasmon resonance · template

Noble metal nanostructures can interact strongly with the visible light through the resonant excitation of the collective oscillations of their conduction electrons, namely surface plasmon resonance.[1,2] Surface plasmons have been used to enhance the surface sensitivity of several spectroscopic techniques including fluorescence spectroscopy,[3,4] Raman scattering,[5] and second harmonic generation.[6,7] Surface plasmons can also be usefully exploited for subwavelength optical waveguides,[8,9] biolabeling,[10] and chemical and biological sensing.[11,12] It has been demonstrated theoretically and experimentally that the strength and wavelength of the surface plasmon resonance strongly depend on the geometry, size, and surrounding environment of a metal nanostructure.[1,13−16] Therefore, the ability to tailor and tune these parameters is of essential importance to adjust the plasmonic behavior to meet the desired application. Recently, several groups reported on the preparation of crescent-shaped Au nanostructures, which exhibit attractive optical properties and lead to local electromagnetic field enhancement resulting from their sharp corners.[17−21] The applied synthetic methods were mostly based on electron beam lithography (EBL), focused ion beam (FIB), and sphere lithography. EBL and FIB are costly processes with limited yields.[6,19,22,23] Nanosphere lithography[24−26] and shadow-based nanofabrication[27,28] have demonstrated a promising potential to alleviate some of the challenges facing large-scale synthesis of thin crescent-shaped nanostructures.

In this work, we demonstrate a flexible template-based approach for the synthesis of sharp-edged (below 5 nm curvature radius) crescent-shaped half-nanotubes (HNTs). Their plasmonic properties are also investigated by dark field scattering and surface enhanced Raman scattering. Our method relies initially on the creation of crescent-shaped nanochannels in an anodic aluminum oxide (AAO) template by removal of a sacrificial layer coated onto the pore walls by atomic layer deposition (ALD). Subsequent electrodeposition of metal into the nanochannels produces the desired metal nanostructures. This method provides a precise, convenient, flexible size and shape control. A schematic illustration of the preparation process is displayed in Figure 1. At first, a ZnO layer is deposited onto the pore walls of an AAO template by ALD. Subsequently, the remaining space of these pores is completely filled with Al_2O_3 also deposited by ALD. In this work we have selected ZnO and Al_2O_3 as sacrificial and filling materials, respectively, because their deposition processes are well-established and show high deposition rates and good quality. In addition, ZnO can be selectively removed by wet-chemical etching. After ion milling removal of ZnO and Al_2O_3 layers from both the top and bottom sides of the

*Address correspondence to yqin@mpi-halle.de, mknez@mpi-halle.de.

Received for review July 6, 2010 and accepted December 23, 2010.

Published online January 06, 2011
10.1021/nn102879s

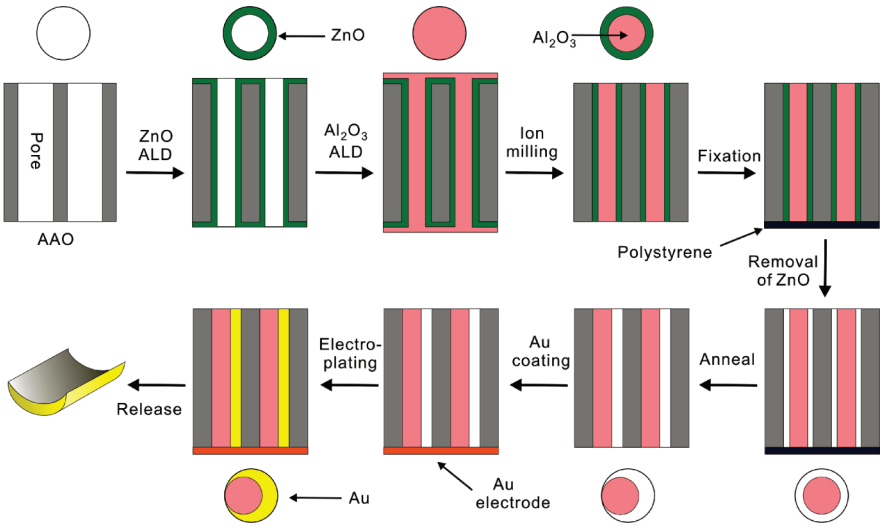

Figure 1. A schematic diagram illustrating the fabrication process of Au crescent-shaped half-nanotubes.

AAO template, dissolved polystyrene is poured onto one side of the template to stabilize the filled Al_2O_3. Subsequently, the remaining ZnO layer covering the pore walls is removed by etching in HNO_3. This procedure leads to a spacing between the Al_2O_3 nanowire-like filling and the pore walls. A template with crescent-shaped nanochannels is created after the removal of polystyrene by annealing the template in air. A thin film of gold is coated on one side of the template by ion sputtering to produce an electrode. Subsequently, electrodeposition is performed to fill the nanochannels with Au, thereby yielding crescent-shaped HNTs. Finally, these HNTs are released by dissolving the template and the Al_2O_3 filling in an aqueous solution of NaOH.

RESULTS AND DISCUSSION

Figure 2a shows the cross-sectional scanning electron microscope (SEM) image of an AAO template with pores of 25 um in depth having their sidewalls coated by a ZnO layer with 40 nm thickness and subsequently filled with Al_2O_3 (500 cycles). The number of ALD cycles needed for Al_2O_3 to ensure an efficient filling depends sensitively on the pore diameter (180 nm) as well as on the thickness of ZnO layers. In this image the ZnO layers show a brighter contrast (thin bright line) when compared to the AAO pore wall and the Al_2O_3 filling at the center. The ZnO is conformally coated onto the entire length of the pore walls, exhibiting one advantage of ALD.[29] The conformal thickness plays an important role in the subsequent production of HNTs with a uniform size and adjustable opening. In addition, it can be seen that both the top and bottom sides of the template are also covered by ZnO and Al_2O_3, which will be removed by ion milling in the subsequent steps of the fabrication process (Figure 1). Figure 2b displays a top-view SEM image of the template after ion milling. The ZnO layers in the pores exhibit circular bright lines after the surface ZnO and Al_2O_3 layers are effectively removed. Figure 2c shows a top-view SEM image of the templates after etching of the ZnO in the pores and removal of the fixing polystyrene by annealing. In this way, instead of circular nanochannels, crescent-shaped nanochannels are successfully produced, resulting from the displacement of the Al_2O_3 nanowires and their attachment to the pore walls as a result of the absence of the support. A cross-sectional SEM image of a cleaved template with nanochannels is shown in Figure 2d. The Al_2O_3 nanowires and also the spacing between the nanowires and the pore walls are clearly observed.

After the electrodeposition of Au into the nanochannels, a cross-sectional sample of the template was prepared by ion beam milling, as shown in Figure 3a. Au shows an apparently brighter contrast compared to their surroundings, clearly revealing a crescent-shaped cross-section. The nanostructures display sharp edges, consistent with the starting nanochannels. Figure 3b shows the freestanding crescent-shaped HNT arrays released by dissolving the template and the Al_2O_3 filling (nanowires) in an aqueous NaOH solution. These HNTs have a typical length of up to 10 μm, depending on the electrodeposition time. Figure 3c is a top view SEM image of the HNT arrays at a higher magnification, while Figure 3d is a close-up SEM image of the body of the HNTs. Their external diameters are about 180 nm, consistent with the initial pore sizes of the template. Both the outer and inner surfaces appear to be relatively smooth. The crescent-shaped profile and opening along the entire length of the HNTs could clearly be observed. This indicates that the resulting HNTs mimic the shape of the initial nanochannels very well.

The opening of the HNTs relies on the thickness of the initial sacrificial ZnO layer and can thus be conveniently controlled by varying the number of ZnO ALD cycles, as schematically shown in Figure 4a. Expectedly, the

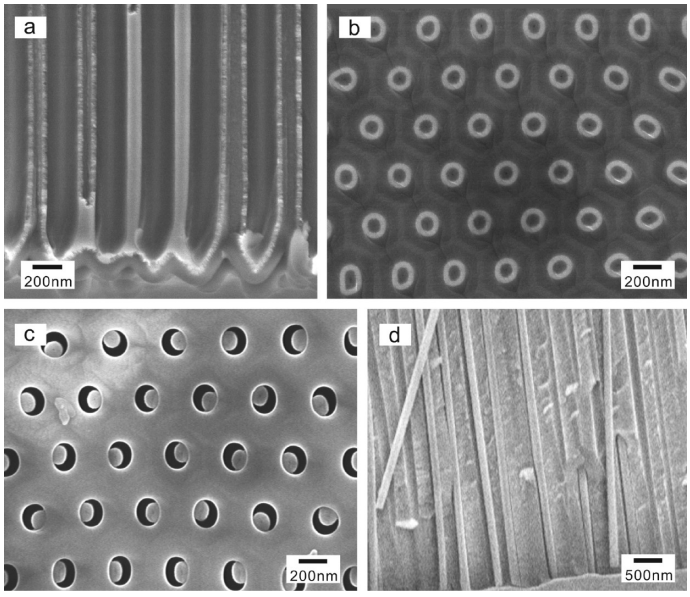

Figure 2. (a) Cross-sectional SEM image of an AAO template after ALD of ZnO (250 cycles, 40 nm), followed by Al_2O_3 filling (500 cycles). (b) Top-view SEM image of the template after ion milling. (c, d) Top-view and cross-sectional SEM images of the template after etching of ZnO and removal of polystyrene.

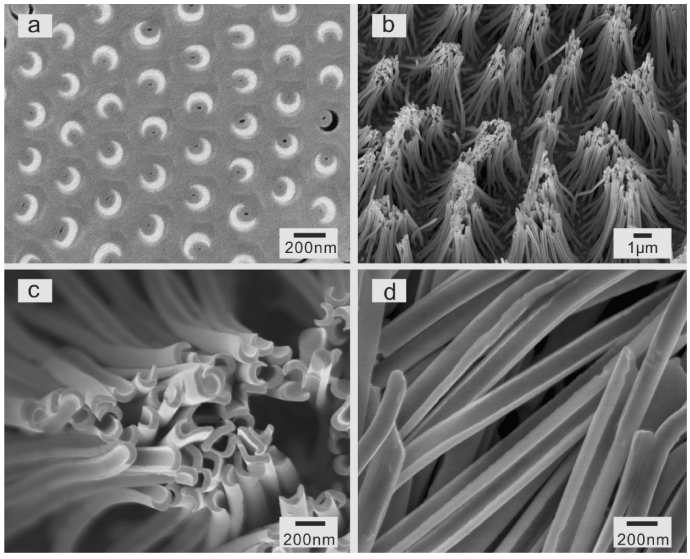

Figure 3. (a) Cross-sectional SEM image of an AAO template after electrodeposition of Au into the crescent-shaped nanochannels created with a 40 nm-thick ZnO sacrificial layer. (b, c) Top-view SEM images of the HNT arrays released by dissolving the template and Al_2O_3 filling materials in a NaOH aqueous solution. (d) A close-up of the HNTs.

maximum thickness of the HNTs is twice that of the initial ZnO layer. Figure 4b shows a SEM image of Au HNTs obtained by electrodeposition of Au within the nanochannels created with a 60 nm ZnO layer. The maximum thickness of the tube walls is about 120 nm and the gap between the two edges is about 80 nm. By decreasing the thickness of the ZnO layer to 40 nm, crescent-shaped HNTs are also obtained (Figure 4c), as depicted in Figure 3. They have a wall thickness of about 80 nm, in addition to lager opening, wider gap, and sharper edges. However, their external diameter remains the same (~180 nm) as restricted by the pore diameter of the template. When the thickness of the ZnO layer is further reduced to 15 nm, HNTs with much thinner thickness (30 nm), wider gap size, and larger opening are produced as shown in Figure 4d. The curvature radius of their edges can be below 5 nm. It should be mentioned that HNTs with tunable external diameters could also be conveniently fabricated by depositing an Al_2O_3 layer onto the pore walls of the templates before the deposition of ZnO to reduce the pore diameters or using AAO templates with different initial pore sizes.

To investigate the surface plasmon behavior of the obtained nanostructures, optical scattering spectra

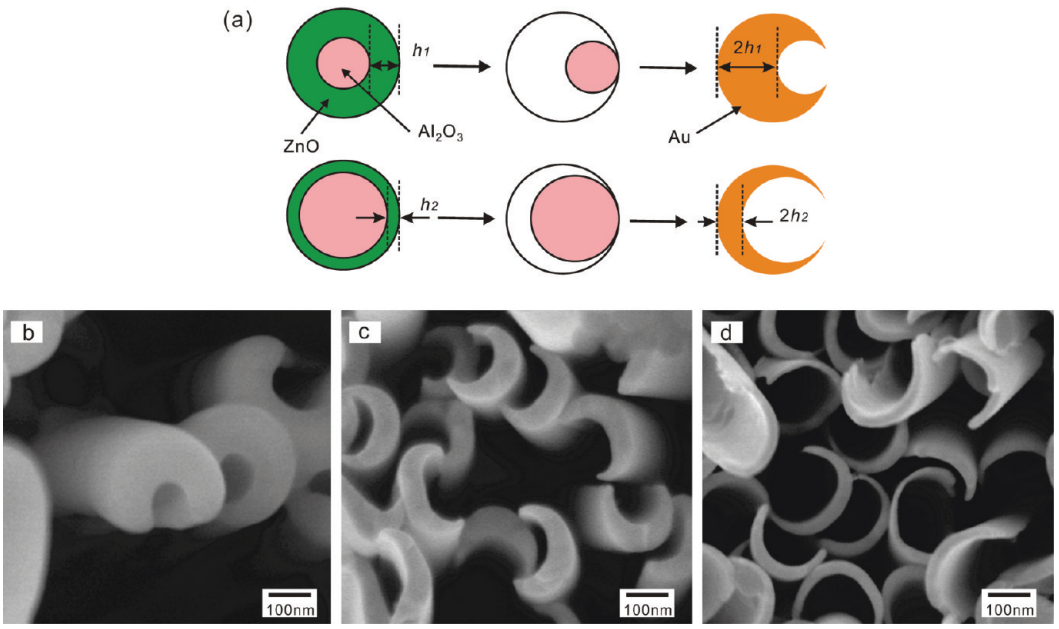

Figure 4. (a) Schematic illustration showing tunable opening, thickness, gap size, and edge sharpness of the crescent-shaped HNTs depending on the thickness (*h*) of the initial sacrificial ZnO. (b−d) High-magnification SEM images of HNTs obtained from ZnO thicknesses of 60, 40, and 15 nm, respectively.

were measured by dark field confocal microscopy. When the epi-illumination works on the dark field mode, the scattering light is coupled into a visible and near-infrared (Vis-NIR) spectrometer equipped with a liquid nitrogen cooled CCD detector. A small aperture is placed at the intermediate image plane to spatially filter the collected light to an area of 20 μm diameter on the sample plane. This dark field illumination maximizes the scattering from the nanostructures, and minimizes the background scattering from the substrate.[30,31] The scattering efficiency is corrected for wavelength dependence of the lamp emission and the system response by replacing the sample with a silver mirror and collecting the reflected light in the bright field illumination mode.

The typical scattering spectra of HNTs are shown in Figure 5. For the HNT having a length of 5.6 μm and a thickness of 80 nm, two resonance peaks at 575 and 860 nm are present in its spectrum. For comparison, the scattering spectrum of HNTs with 80 nm thickness embedded in the Al_2O_3 matrix was also determined. Unlike the single HNT spectrum, there is only one distinct resonance peak at 810 nm in the long wavelength range from this spectrum. By comparing these spectra, it can be inferred that for the released HNTs two different resonance modes are excited by the two electrical field components of the incident electrical field projected along the long and short axes of the HNT, respectively. The right peak at 860 nm corresponds to the long axis (longitudinal) mode, while the left peak at 575 nm corresponds to the short axis (transverse) mode.[30−33] However, for these embedded HNTs, the resonance excitation in the short axis mode is highly suppressed, showing a very weak shoulder

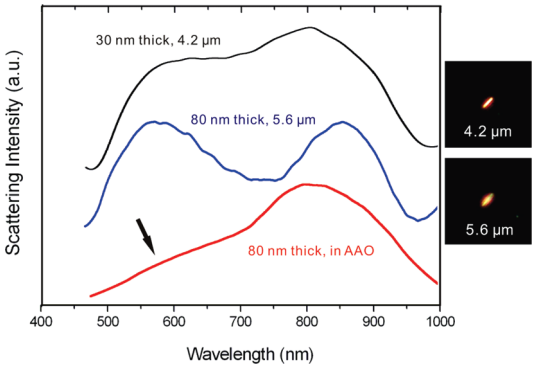

Figure 5. Measured scattering spectra of HNTs having a thickness of 80 nm embedded in AAO as exampled in Figure 3a (red) or distributed on a Si substrate (blue) and having a thickness of 30 nm distributed on a Si substrate (black). Insets show the optical microscopic pictures of these single HNTs distributed on Si substrates taken with a digital camera. These HNTs are prepared by using a template with 180 nm pore diameter.

peak in the short wavelength side as indicated by the arrow. This is not surprising given the fact that both their outer and inner surfaces and especially their sharp edges are covered by Al_2O_3 with only the ends exposed in the air. The blue-shift of the long axis resonance peak from 860 to 810 nm can possibly be ascribed to the high dielectric background of the surrounding Al_2O_3. In addition, the surface plasmon coupling between the HNTs should also be taken into consideration for the blue-shift since the distance between these HNTs is only about 200 nm (Figure 3a) and therefore much smaller than the excitation wavelength.[34,35]

The scattering spectrum of a HNT with a thickness of 30 nm and a length of 4.2 um is also shown in Figure 5.

Two resonance peaks significantly overlap, unlike the clearly separated resonance peaks in the spectrum of single HNTs with thicknesses of 80 nm. By comparing the spectra of HNTs with different thicknesses, it can be derived that the plasmon resonance is sensitive to their geometry. Therefore, it is possible to tailor their optical properties for specific applications by controlling their geometry including diameter, length, opening, gap size, thickness, and edge sharpness. This can be realized by changing the pore diameter of the template, electrodeposition time, or the thickness of the sacrificial ZnO layers as mentioned above. Further near-field optical characterizations and theoretical calculations are necessary to obtain more detailed and complete information on the optical properties of these HNTs, including possible Fabry−Pérot resonance.[36]

The sharpness of the edges along the whole HNT is one of the interesting features displayed by the structures demonstrated in this work. When exposed to a laser having the appropriate wavelength, this morphology should induce a strong enhancement in the local electromagnetic field due to the surface plasmon resonance.[5] The uniformity as well as the high density of these structures makes the exploitation of this phenomenon suitable for molecular spectroscopy. As a prototypical system, we demonstrate here the influence of the enhancement near the sharp edges on Raman vibrational modes of crystal violet (CV) molecules adsorbed on the released HNT sample with a thickness of 80 nm (Figure 3b). Figure 6 displays a typical Raman spectrum in the wavenumber region of ~1500−1675 cm^{-1}. In the investigated wavenumber region, the CV spectrum is characterized by three main peaks centered at ~1528, ~1589, and 1618 cm^{-1}. The peak positions are determined by *voigt* function fits. Independent of the frequency, a strong enhancement of the Raman spectra of CV is observed. For the sake of comparison, spectra recorded for CV molecules adsorbed on the cross-section of Au HNTs still buried in an AAO template (Figure 3a) and Au-sputtered Si substrate are also shown. Note that no peak is detectable for the sample with CV molecules adsorbed on Au-sputtered substrate. While still buried in the AAO template, the emerging corners of HNTs (Figure 3a) induce a clear enhancement comparable to what can be achieved by using Au nanoparticles with a comparable density and size. To highlight the unique plasmonic behavior of the HNTs, we prepared an additional set of samples. CV molecules were adsorbed on solid Au nanowires (NWs) having a diameter and length comparable to those of Au-HNTs. Aside the omitted filling step of the template, the NWs were produced with identical experimental conditions. A representative Raman spectrum recorded for this set of specimens is also displayed in Figure 6. Interestingly, in contrast to the spectrum recorded using released Au HNTs exhibiting a substantial increase in the intensity of CV

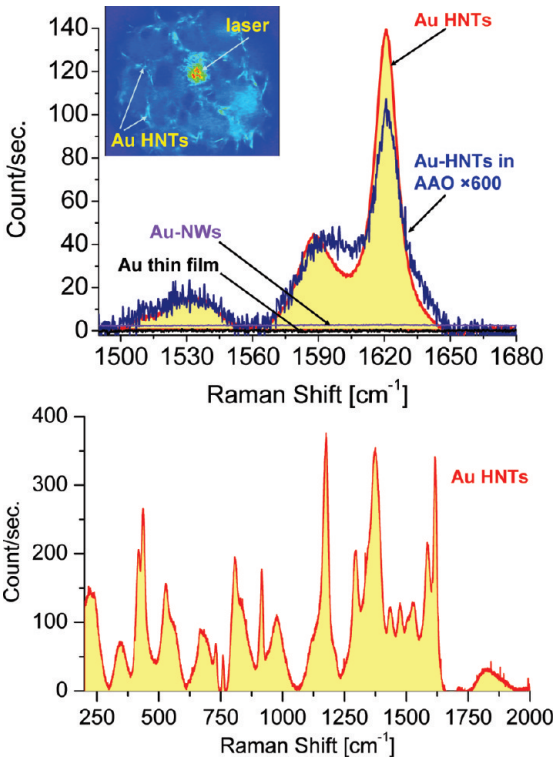

Figure 6. Surface enhanced Raman scattering spectra of CV molecules adsorbed on Au HNTs (red line), on Au HNTs still buried in AAO (blue line), on Au-sputtered Si substrate (black line), and on Au NWs (violet line). Inset: 50 μm × 50 μm optical image of the surface of the HNT sample exposed to a 633 nm laser during micro-Raman analysis. Bottom: The 200−2000 cm^{-1} range of CV molecule Raman spectrum recorded on Au HNTs. For comparison, the signal obtained with Au HNTs still embedded in AAO is amplified by a factor of 600.

Raman peaks, no clear Raman signal is, however, observed for CV molecules adsorbed on the Au NW samples. Obviously, the strong Raman signal obtained from released HNTs is a direct manifestation of the excitation of surface plasmons on the sharp edges of Au HNTs. In the present case, the enhancement obtained with HNTs is ~600× larger than what it is typically obtained from the cross-sectional samples of HNTs still buried in AAO (*i.e.*, a two-dimensional SERS substrate). Note, however, that the larger enhancement using released HNTs compared to HNTs still buried in the AAO should not only be associated with the increase in the exposed area of Au HNTs. In fact, the increase in the exposed area *per se* has no large effect on SERS signal since the field enhancement drops as a function of r^{-N}, where r is the distance from the sharp edge. In the simple and well-investigated case of plasmonic nanoparticles N amounts to 10.[37] However, it is well-known that the electromagnetic mechanisms of SERS are strongly sensitive to size, shape, and spatial distribution of the scattering nanoobjects.[38] A clear description of the power law governing the field enhancement for our HNTs is still missing, but one may expect N to be ~1 in analogy to recent SERS studies in one-dimensional nanostructures.[39−43] Thus

the larger enhancement of the Raman signal for the released HNT sample is due to the increase in plasmonic hot spots (*i.e.*, sharp edges) associated with the geometry of HNTs.

CONCLUSIONS

In summary, we have demonstrated a flexible and versatile method for producing aligned crescent-shaped HNTs. This was achieved by electrodeposition inside crescent-shaped nanochannels created by removal of a sacrificial layer, which was deposited by ALD onto the pore walls of an AAO template. This method allows convenient control over the edge sharpness, opening, gap size, diameter, and the wall thickness of the HNTs. Initial investigations of the dark field scattering and surface enhanced Raman scattering reveal distinct surface plasmon resonance on the sharp edge of the Au HNTs in the visible and infrared regions. Our method creates a wealth of opportunities to generate HNTs of a variety polymers and other inorganic materials, provided that they can be electrodeposited. Moreover modulated HNTs could be synthesized by alternating the electrodeposition of different materials within the crescent-shaped nanochannels. The HNTs promise application potential in chemical and biological sensing, as optical antennas, ultra sensitive Raman, or further emerging fields. Finally, it is important to mention that HNTs still embedded in AAO (corresponding to Au nanocrescents) could be potentially employed in the fields of metamaterials provided a precise control of their orientation can be achieved, which remains a formidable challenge but not insurmountable.

EXPERIMENTAL SECTION

Self-ordered AAO templates with a pore diameter of 180 nm and a pore depth of 25 μm were prepared by electrochemical anodization.[44] ALD was carried out in a commercial hot-wall flow-type ALD reactor (SUNALE R75, Picosun, Finland) utilizing N_2 as a precursor carrier and purge gas at a pressure of 10 Torr. Deposition of Al_2O_3 was performed with $Al(CH_3)_3$ and deionized H_2O as precursors at a growth rate of 1.0 Å per cycle and 150 °C. $Zn(C_2H_5)_2$ and deionized water were used as precursors for ZnO deposition at a deposition rate of 1.6 Å per cycle at 100 °C.

After ALD, ion milling was performed for sufficient time by an argon-ion-beam milling system (Duo mill 600 DIF, GATAN) to remove ZnO and Al_2O_3 layers on both sides of the coated AAO templates. Polystyrene solution in chloroform (20%) was dropped onto one side of the milled template for fixation. After evaporation of the solvent, the sacrificial ZnO layers in the pores were removed by etching with concentrated HNO_3 (60 wt %) for 20 min at room temperature. Then the templates were washed with H_2O. To remove the polystyrene, annealing was performed at 550 °C for 1 h in air using a tube furnace.

The gold HNTs were electrodeposited at a constant current density of 1 mA/cm^2 with a commercial gold plating solution (Orotemp, Technic Inc.) as the electrolyte. The electrodeposition was carried out at room temperature and the typical deposition time was 20 min. To release the HNTs from the templates, the Al_2O_3 filling and also the AAO templates were removed with 4 M NaOH at 45 °C for 6 h. For the scattering spectra analysis, the released HNTs were dispersed in ethanol by ultrasonication for 10 s. Several drops of the suspension were dropped onto a Si wafer, which was allowed to dry at ambient temperature.

Raman analysis was carried out in backscattering geometry using a Horiba Jobin Yvon LabRam HR 800 nm high-resolution Raman microscope. In this setup, the Raman signal was acquired by a thermoelectrically cooled CCD array detector. A HeNe laser line operating at 633 nm was used as the excitation source. The laser spot on the sample surface was ~1 μm in diameter. To avoid any local heating effects, the laser power was kept below 0.3 mW. The accumulation time was 10 s. About 1024 spectra were recorded from a 50 μm × 50 μm region (inset in Figure 6) for each sample. The collected spectra were processed using the LabSpec program. Surface-enhanced Raman scattering CV specimens were prepared by exposing the samples to 10^{-5} molar aqueous CV for 15 min after wet chemical cleaning, and then rinsed with deionized water.

Solid Au NWs with a diameter and length comparable to those of Au HNTs were also prepared by electrodeposition using an AAO template with a similar pore diameter (180 nm). For comparison, released Au NWs were used for Raman scattering investigations.

Acknowledgment. This work is dedicated to the memory of Prof. Ulrich Gosele. This work was financially supported by the German Federal Ministry of Education and Research (BMBF) with the contract number FKZ: 03X5507. A.P. is grateful to the NSF of China (term nos. 90923014 and 10974050) for financial support. We also acknowledge the ion milling work by Sigrid Hopfe.

REFERENCES AND NOTES

1. Bohren, C. F.; Huffman, D. R. *Absorption and Scattering of Light by Small Particles*; Wiley: New York, 1983.
2. Kreibig, U.; Vollmer, M. *Optical Properties of Metal Clusters*; Springer: Berlin, Germany, 1995; Vol. 25.
3. Lakowicz, J. R.; Geddes, C. D.; Gryczynski, I.; Malicka, J.; Gryczynski, Z.; Aslan, K.; Lukomska, J.; Matveeva, E.; Zhang, J.; Badugu, R.; *et al.* Advances in Surface-Enhanced Fluorescence. *J. Fluoresc.* **2004,** *14*, 425–441.
4. Xie, X. S. Single-Molecule Spectroscopy and Dynamics at Room Temperature. *Acc. Chem. Res.* **1996,** *29*, 598–606.
5. Nie, S. M.; Emery, S. R. Probing Single Molecules and Single Nanoparticles by Surface-Enhanced Raman Scattering. *Science* **1997,** *275*, 1102–1106.
6. Lamprecht, B.; Leitner, A.; Aussenegg, F. R. SHG Studies of Plasmon Dephasing in Nanoparticles. *Appl. Phys. B: Lasers Opt.* **1999,** *68*, 419–423.
7. Klein, M. W.; Enkrich, C.; Wegener, M.; Linden, S. Second-Harmonic Generation from Magnetic Metamaterials. *Science* **2006,** *313*, 502–504.
8. Maier, S. A.; Kik, P. G.; Atwater, H. A.; Meltzer, S.; Harel, E.; Koel, B. E.; Requicha, A. A. G. Local Detection of Electromagnetic Energy Transport Below the Diffraction Limit in Metal Nanoparticle Plasmon Waveguides. *Nat. Mater.* **2003,** *2*, 229–232.
9. Quinten, M.; Leitner, A.; Krenn, J. R.; Aussenegg, F. R. Electromagnetic Energy Transport *via* Linear Chains of Silver Nanoparticles. *Opt. Lett.* **1998,** *23*, 1331–1333.
10. Schultz, S.; Smith, D. R.; Mock, J. J.; Schultz, D. A. Single-Target Molecule Detection with Nonbleaching Multicolor Optical Immunolabels. *Proc. Natl. Acad. Sci. U.S.A.* **2000,** *97*, 996–1001.
11. Cao, Y. C.; Jin, R.; Mirkin, C. A. Nanoparticles with Raman Spectroscopic Fingerprints for DNA and RNA Detection. *Science* **2002,** *297*, 1536–1540.
12. Hirsch, L. R.; Jackson, J. B.; Lee, A.; Halas, N. J.; West, J. L. A Whole Blood Immunoassay Using Gold Nanoshells. *Anal. Chem.* **2003,** *75*, 2377–2381.
13. Kreibig, U.; Genzel, L. Optical Absorption of Small Metallic Particles. *Surf. Sci.* **1985,** *156*, 678–700.

14. Link, S.; El-Sayed, M. A. Spectral Properties and Relaxation Dynamics of Surface Plasmon Electronic Oscillations in Gold and Silver Nanodots and Nanorods. *J. Phys. Chem. B* **1999,** *103*, 8410–8426.
15. Sönnichsen, C.; Geier, S.; Hecker, N. E.; von Plessen, G.; Feldmann, J.; Ditlbacher, H.; Lamprecht, B.; Krenn, J. R.; Aussenegg, F. R.; Chan, V. Z. H.; *et al.* Spectroscopy of Single Metallic Nanoparticles Using Total Internal Reflection Microscopy. *Appl. Phys. Lett.* **2000,** *77*, 2949–2951.
16. Kottmann, J. P.; Martin, O. J. F.; Smith, D. R.; Schultz, S. Dramatic Localized Electromagnetic Enhancement in Plasmon Resonant Nanowires. *Chem. Phys. Lett.* **2001,** *341*, 1–6.
17. Lu, Y.; Liu, G. L.; Kim, J.; Mejia, Y. X.; Lee, L. P. Nanophotonic Crescent Moon Structures with Sharp Edge for Ultrasensitive Biomolecular Detection by Local Electromagnetic Field Enhancement Effect. *Nano Lett.* **2005,** *5*, 119–124.
18. Shumaker-Parry, J. S.; Rochholz, H.; Kreiter, M. Fabrication of Crescent-Shaped Optical Antennas. *Adv. Mater.* **2005,** *17*, 2131–2134.
19. Li, K.; Clime, L.; Cui, B.; Veres, T. Surface enhanced Raman scattering on long-range ordered noble-metal nanocrescent arrays. *Nanotechnology* **2008,** *19*, 145305.
20. Wu, L. Y.; Ross, B. M.; Lee, L. P. Optical Properties of the Crescent-Shaped Nanohole Antenna. *Nano Lett.* **2009,** *9*, 1956–1961.
21. Choi, Y.; Hong, S.; Lee, L. P. Shadow Overlap Ion-beam Lithography for Nanoarchitectures. *Nano Lett.* **2009,** *9*, 3726–3731.
22. Linden, S.; Enkrich, C.; Wegener, M.; Zhou, J. F.; Koschny, T.; Soukoutis, C. M. Magnetic Response of Metamaterials at 100 Terahertz. *Science* **2004,** *306*, 1351–1353.
23. Fromm, D. P.; Sundaramurthy, A.; Schuck, P. J.; Kino, G.; Moerner, W. E. Gap-Dependent Optical Coupling of Single "Bowtie" Nanoantennas Resonant in the Visible. *Nano Lett.* **2004,** *4*, 957–961.
24. Hulteen, J. C.; Van Duyne, R. P. Nanosphere Lithography: A Materials General Fabrication Process For Periodic Particle Array Surfaces. *J. Vac. Sci. Technol., A* **1995,** *13*, 1553–1558.
25. Kosiorek, A.; Kandulski, W.; Chudzinski, P.; Kempa, K.; Giersig, M. Shadow Nanosphere Lithography: Simulation And Experiment. *Nano Lett.* **2004,** *4*, 1359–1363.
26. Charnay, C.; Lee, A.; Man, S.-Q; Moran, C. E.; Radloff, C.; Bradley, R. K.; Halas, N. J. Reduced Symmetry Metallodielectric Nanoparticles: Chemical Synthesis and Plasmonic Properties. *J. Phys. Chem. B* **2003,** *107*, 7327–7333.
27. Hanarp, P.; Käll, M.; Sutherland, D. S. Optical Properties of Short Range Ordered Arrays of Nanometer Gold Disks Prepared by Colloidal Lithography. *J. Phys. Chem. B* **2003,** *107*, 5768–5772.
28. Aizpurua, J.; Hanarp, P.; Sutherland, D. S.; Käll, M.; Bryant, G. W.; de Abajo, F. J. G. Optical Properties of Gold Nanorings. *Phys. Rev. Lett.* **2003,** *90*, 057401.
29. Knez, M.; Nielsch, K.; Niinistö, L. Synthesis and Surface Engineering of Complex Nanostructures by Atomic Layer Deposition. *Adv. Mater.* **2007,** *19*, 3425–3438.
30. Xu, Q.; Bao, J.; Capasso, F.; Whitesides, G. Surface Plasmon Resonances of Free-Standing Gold Nanowires Fabricated by Nanoskiving. *Angew. Chem., Int. Ed.* **2006,** *45*, 3631–3635.
31. Wei, Q. H.; Su, K. H.; Durant, S.; Zhang, X. Plasmon Resonance of Finite One-Dimensional Au Nanoparticle Chains. *Nano Lett.* **2004,** *4*, 1067–1071.
32. Ditlbacher, H.; Krenn, J. R.; Lamprecht, B.; Leitner, A.; Aussenegg, F. R. Spectrally Coded Optical Data Storage by Metal Nanoparticles. *Opt. Lett.* **2000,** *25*, 563–565.
33. Hutter, E.; Fendler, J. H. *Adv. Mater.* **2004,** *16*, 1685–1706.
34. Rechberger, W.; Hohenau, A.; Leitner, A.; Krenn, J. R.; Lamprecht, B.; Aussenegg, F. R. Optical Properties of Two Interacting Gold Nanoparticles. *Opt. Commun.* **2003,** *220*, 137–141.
35. Lassiter, J. B.; Aizpurua, J.; Hernandez, L. I.; Brandl, D. W.; Romero, I.; Lai, S.; Harfner, J. H.; Nordlander, P.; Halas, N. J. Close Encounters between Two Nanoshells. *Nano Lett.* **2008,** *8*, 1212–1218.
36. Esteban, R.; Vogelgesang, R.; Dorfmuller, J.; Dmitriev, A.; Rockstuhl, C.; Etrich, C.; Kern, K. Direct Near-Field Optical Imaging of Higher Order Plasmonic Resonances. *Nano Lett.* **2008,** *8*, 3155–3159.
37. Stiles, P. L.; Dieringer, J. A.; Shah, N. C.; Van Duyne, R. P. Surface-Enhanced Raman Spectroscopy. *Annu. Rev. Anal. Chem.* **2008,** *1*, 601–626.
38. Du, Y.; Shi, L.; He, T.; Sun, X.; Mo, Y. SERS Enhancement Dependence on the Diameter and Aspect Ratio of Silver-Nanowire Array Fabricated by Anodic Aluminium Oxide Template. *Appl. Surf. Sci.* **2008,** *255*, 1901–1905.
39. Mo, Y.; Mörke, I.; Wachter, P. The Influence of Surface-Roughness on the Raman-Scattering of Pyridine on Copper and Silver Surfaces. *Solid State Commun.* **1984,** *50*, 829–832.
40. Su, K. H.; Wei, Q. H.; Zhang, X.; Mock, J. J.; Smith, D. R.; Schultz, S. Interparticle Coupling Effects on Plasmon Resonances of Nanogold Particles. *Nano Lett.* **2003,** *3*, 1087–1090.
41. Liao, Q.; Mu, C.; Xu, D.-S.; Ai, X.-C.; Yao, J.-N.; Zhang, J.-P. Gold Nanorod Arrays with Good Reproducibility for High-Performance Surface-Enhanced Raman Scattering. *Langmuir* **2009,** *25*, 4708–4714.
42. Liu, Y.-J.; Zhang, Z.-Y.; Zhao, Q.; Dluhy, R. A.; Zhao, Y.-P. The Role of the Nanospine in the Nanocomb Arrays for Surface Enhanced Raman Scattering. *Appl. Phys. Lett.* **2009,** *94*, 033103.
43. Liu, Y.-J.; Zhang, Z.-Y.; Dluhy, R. A.; Zhao, Y.-P. The SERS Response of Semiordered Ag Nanorod Arrays Fabricated by Template Oblique Angle Deposition. *J. Raman Spectrosc.* **2010,** *40*, 1112–1118.
44. Liu, L.; Lee, W.; Huang, Z.; Scholz, R.; Gösele, U. Fabrication and Characterization of A Flow-Through Nanoporous Gold Nanowire/AAO Composite Membrane. *Nanotechnology* **2008,** *19*, 335604.